Conference on Modelling Fluid Flow (CMFF'25)
The 19th International Conference on Fluid Flow Technologies
Budapest, Hungary, August 26 - August 29, 2025

BEM SIMULATION OF AN EXPANDING / CONTRACTING BUBBLE IN VISCOELASTIC FLUIDS

Koki Asano[1], Honami Nishimura[2], Haruki Furukawa[3],
Tim Phillips[5], Steven Lind[6], Shuichi Iwata[4]

[1] Department of Life-Science and Applied Chemistry, Graduate School of Engineering, Nagoya Institute of Technology, Gokiso-cho, Showa-ku, Nagoya, Aichi, 466-8555, Japan. Tel: +81-52-735-5256, Fax: +81-52-735-5255, E-mail: k.asano.057@nitech.ac.jp
[2] Department of Life-Science and Applied Chemistry, Graduate School of Engineering, Nagoya Institute of Technology, Gokiso-cho, Showa-ku, Nagoya, Aichi, 466-8555, Japan, E-mail: h.nishimura.929@nitech.jp
[3] Department of Life-Science and Applied Chemistry, Graduate School of Engineering, Nagoya Institute of Technology, Gokiso-cho, Showa-ku, Nagoya, Aichi, 466-8555, Japan, E-mail: furukawa.haruki@nitech.ac.jp
[4] Corresponding Author. Department of Life-Science and Applied Chemistry, Graduate School of Engineering, Nagoya Institute of Technology, Gokiso-cho, Showa-ku, Nagoya, Aichi, 466-8555, Japan, E-mail: iwa@nitech.ac.jp
[5] School of Mathematics, Cardiff University, E-mail: PhillipsTN@cardiff.ac.uk
[6] School of Engineering, Cardiff University, E-mail: LindS1@cardiff.ac.uk

ABSTRACT

We measured motion of rising bubble under pressure-oscillating field, and reported a significant enhancement of the rising velocity up to approximately 400 times for a shear-thinning fluid with 1–5 mm^3 bubbles in 0.8 wt% aqueous sodium polyacrylate (SPA) (Iwata *et al.* JNNFM, 2008). Complex local flow is observed as uniaxial extension occurred at the tail of the bubble during the contraction phase as well as the biaxial extensional deformation occurred at the upper side of the bubble (Iwata *et al*., JNNFM, 2019). To analyze the flow near the bubble, Ito *et al*. analyzed the motion of an expanding/contracting rising bubble in the Carreau-Yasuda model fluid by FEM analysis (Reoroji Gakkaishi, 2020). However, the FEM analysis didn't take into account the effect of viscoelasticity of surrounding fluid.

Therefore, we applied the boundary element method (BEM) to the problem of an expanding/contracting bubble and modelled the fluid external to the bubble as a viscoelastic fluid. The bubble is initially located near a rigid wall. In this study, the Giesekus model is used as a viscoelastic model. We aim to clarify the influence of the rigid wall on the deformation and dynamics of an expanding/contracting bubble.

Keywords: Deformation, Boundary Element Method, Viscoelastic fluid, Rigid wall, Giesekus model

NOMENCLATURE

h	[-]	non-dimensional position of bubble center
P_b	[Pa]	pressure of bubble
P_0	[Pa]	initial bubble pressure
P_{ref}	[Pa]	pressure of viscoelastic fluid
$\dot{\gamma}$	[s^{-1}]	shear rate
η	[Pa·s]	shear viscosity
η_0	[Pa·s]	zero-shear viscosity
η_p	[Pa·s]	viscosity of polymer solutions
η_s	[Pa·s]	solvent viscosity
η_e	[Pa·s]	extensional viscosity
$\dot{\varepsilon}$	[s^{-1}]	elongation velocity
N_1	[Pa]	first normal stress difference
λ_1	[s]	relaxation time
λ_2	[s]	delay time
μ	[Pa·s]	viscosity of viscoelastic fluid
ρ	[kg/m^3]	density of viscoelastic fluid
γ	[J/(kg·K)]	specific heat
ω	[rad/s]	angular frequency
G'	[Pa]	storage modulus
G''	[Pa]	loss modulus
T	[Pa]	extra stress
n	[-]	subscript indicating the normal direction
$T_{nn}{}^p$	[Pa]	the normal-normal component of stress T in the polymeric part
σ	[N/m]	surface tension
C	[m^{-1}]	curvature
∇	[m^{-1}]	gradient operator
V	[m^3]	bubble volume
V_0	[m^3]	initial bubble volume
R_0	[m]	initial bubble radius
R_m	[m]	maximum bubble radius

r	[m]	r-coordinate
z	[m]	z-coordinate
t	[s]	time
$\mathbf{x}$	[-]	position vector
$\mathbf{u}$	[-]	irrotational velocity vector
$\mathbf{S}$	[s^{-1}]	rate of strain of tensor
α	[-]	Giesekus model parameter
Re	[-]	Reynolds number
De	[-]	Deborah number
We	[-]	Weber number
N_b	[-]	number of nodes on the bubble
k	[-]	nodal number
ϕ	[-]	dimensionless velocity potential
r^*	[-]	dimensionless r-coordinate
z^*	[-]	dimensionless z-coordinate
t^*	[-]	dimensionless time
E	[-]	ratio of the solvent viscosity to the zero-shear viscosity

1. INTRODUCTION

A tiny air bubble in viscoelastic fluid moves upward at a very slow rising velocity due to the fluid viscosity. Thus, the bubble may take a very long time to travel through the fluid. To address this issue, Iwata *et al*. proposed the Pressure-Oscillation Deforming (POD) method.

This method involves applying pressure oscillations from the vessel to the fluid containing bubbles, which gives rise to alternating expansion and contraction of the bubbles. The cyclical change in bubble diameter due to pressure oscillations generates strong, continuous local flows and shear near the bubble, giving rise to lower local viscosity in the case of shear-thinning fluids. This viscosity reduction significantly accelerates the bubble rise velocity up to more than 400 times in the case of 1–5 mm³ bubbles in a 0.8 wt% aqueous sodium polyacrylate (SPA) solution (zero-shear viscosity η_0 = 90 Pa·s) [1]. The experimental snapshots indicate that the bubble forms a spherical shape during the expansion phase and develops a cusped shape at the tail of the bubble during the contraction phase.

To further investigate bubble dynamics, Ito *et al*.[2] performed numerical analysis of the flow around a bubble using the unsteady finite element method. The fluid properties of Carreau-Yasuda model were fitted with experimental data with steady shear measurements of a 0.8 wt% SPA solution by a stress-controlled rheometer. The results showed that in a purely viscous fluid subjected to 1 Hz oscillations from below, the local shear rate increased at the bottom of the bubble during the contraction phase and at the top during the expansion phase. However, under these conditions, it was difficult to observe a cusped bubble, as the elastic effects were not considered in this analysis.

Therefore, the boundary element method (BEM) was considered to quantitatively evaluate the behavior of a bubble in viscoelastic fluids. Lind and Phillips [3] performed BEM analysis of an oscillating bubble near a rigid wall in an infinite space filled with an upper convected Maxwell fluid. In the present study, instead of employing the Maxwell model, we introduced the Giesekus model, which exhibits shear-thinning behavior and increases has a first normal stress difference that increases moderately with increasing shear rate. Additionally, to ensure a realistic representation of the system, we fitted the model's rheological properties to match those of the high-viscosity experimental fluid with zero-shear viscosity η_0 of approximately 90 Pa·s. The numerical modelling in the following sections focuses on the effects of viscoelastic properties on bubble shape, stress distribution, surface tension, and jet velocity dynamics.

2. NUMERICAL ANALYSIS

2.1. Governing Equations

The continuity equation, the momentum equation are expressed by equations (1) to (2), given the following assumptions. The internal energy equation is ignored since there is no heat or mass transfer through the boundary, and temperature is assumed to be constant. Since the fluid is assumed to be incompressible, the fluid density remains constant, and the continuity equation reduces to a velocity constraint. Under this condition, equation (3) is derived. The assumption of irrotationality results in the curl of the velocity vanishing, thus implying the existence of a velocity potential, and the velocity field can be expressed as shown in equation (4). Substituting this into equation (4), it can be seen that this potential satisfies Laplace's equation in the fluid domain. In addition, based on arguments due to Joseph and coworkers (see for example, Joseph and Liao[4]), it is assumed that the viscoelastic effects are only introduced through the boundary conditions, and that the viscosity/rheological effects in the fluid bulk are negligible in this case.

The calculations were performed in a two dimensional cylindrical coordinate system. The initial bubble shape was assumed to be spherical and the bubble center was placed at a distance h, the standoff distance, from the rigid wall. The continuity equations (5), equations of motion (6) and constitutive equations (7) at the bubble surface of the Giesekus model are shown below. The pressure p_b in the bubble is obtained from equation (8). Since the flow inside the fluid is assumed to be potential, the momentum equation can be expressed using the potential ϕ, and equation (6) is obtained by reformulating the Navier–Stokes equation using the velocity potential and including the free-surface stress balance in normal direction at the bubble surface. In addition, equation (7) is the constitutive equation of the Giesekus model, which includes a

nonlinear term to represent shear-thinning behavior.

$$\frac{D\rho}{Dt} + \rho\nabla\cdot\mathbf{u} = 0 \tag{1}$$

$$\rho\frac{D\mathbf{u}}{Dt} = -\nabla P_{ref} + \nabla\cdot\boldsymbol{\tau} \tag{2}$$

$$\nabla\cdot\mathbf{u} = 0 \tag{3}$$

$$\nabla^2\phi = 0 \tag{4}$$

$$\frac{D\mathbf{x}}{Dt} = \nabla\phi \tag{5}$$

$$\rho\frac{D\phi}{Dt} = \frac{\rho}{2}|\mathbf{u}|^2 - 2\eta_s\frac{\partial^2\phi}{\partial n^2} - T_{nn}{}^{p} + \sigma C + P_{ref} - P_0\left(\frac{V_0}{V}\right)^{\gamma} \tag{6}$$

$$\lambda_1\frac{DT_{nn}{}^{p}}{Dt} = -T_{nn}{}^{p} + 2\lambda_1 T_{nn}{}^{p}\frac{\partial^2\phi}{\partial n^2} - \alpha\frac{\lambda_1}{\eta_p}T_{nn}{}^{p2} + 2\eta_p\frac{\partial^2\phi}{\partial n^2} \tag{7}$$

$$P_b = P_0\left(\frac{V_0}{V}\right)^{\gamma} \tag{8}$$

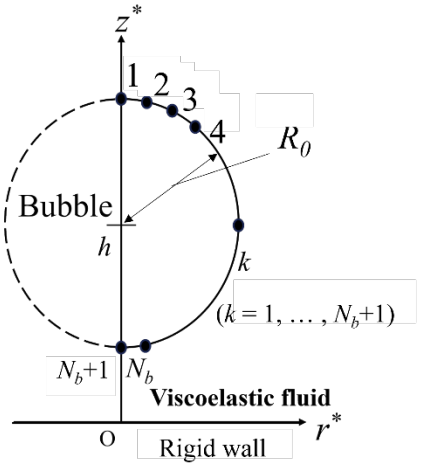

Fig. 1 Schematic diagram of initial conditions when a rigid wall is set up near a bubble.

2.2. Model Set-up

The numerical modelling was performed in a flow field filled with viscoelastic fluid surrounding a single bubble near a rigid wall. As shown in **Fig. 1**, the center of the bubble is initially positioned at a distance h from the rigid wall located at z^*=0, and a two-dimensional axisymmetric flow was assumed with the z-axis in the vertical direction.

2.3. Numerical methods

The bubble surface was discretized into N_b (N_b = 40) segments by distributing N_b+1 nodes on the bubble from the north to south poles of the bubble. Then, the quintic spline representations of the nodal positions (r, z) and potential ϕ were integrated over each interval on the bubble interface using the Gaussian quadrature. The normal stress τ_{nn} is obtained by solving the constitutive equation, and finally, the coordinates (r,z) and the potential ϕ are updated by the fourth-order Runge-Kutta method, respectively.

2.4. Material

The properties of 5 wt% CMC *aq.* measured by a stress-controlled rheometer (MCR302-WESP, Anton Paar, Ltd.) were assumed. Ansys Polymat was used to fit the solution properties to the Giesekus model. The solution density ρ[kg/m^3], initial viscosity η_0, relaxation time λ_1[s], and ratio of the fluid viscosity to the zero-shear viscosity E [-] were determined. A typical value of 1000 kg/cm^3 was used for the density of water. As for the viscoelastic 5wt% CMC solution, the density is ρ = 1049.54 kg/m^3. Zero-shear viscosity η_0 is 90.49 Pa·s.

The viscosity ratio $E = \frac{\eta_s}{\eta_0}$ is obtained as E = 1.105×10^{-5}.

Additionally, two values of the relaxation time λ_1 were considered: λ_1 =0.02 s and λ_1 =10 s. Furthermore, the specific heat ratio γ was set to 1.25, following Walter *et al*.[5].

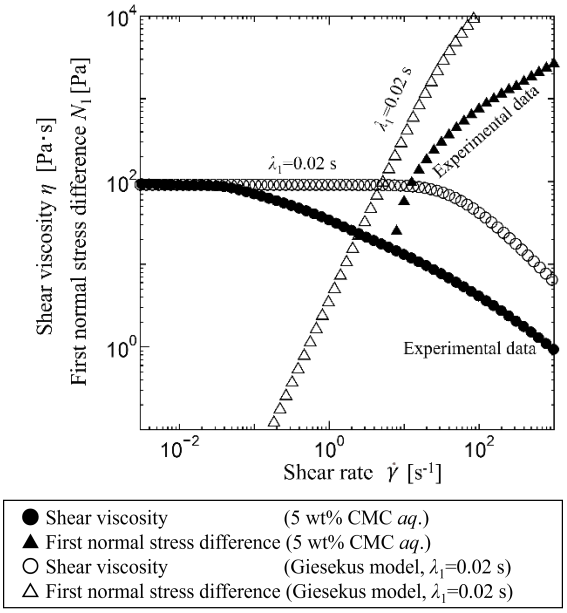

Fig. 2 Profiles of rheological properties of 5 wt% CMC*aq.* and fitting curves of Giesekus model (α = 0.3)

3. RESULTS AND DISCUSSION

We investigated the expansion and contraction phases of a bubble placed near a rigid wall using the Giesekus model (α = 0.3). We analyzed the influence of the initial standoff distance on bubble shape and examined the temporal variations in jet velocity. Furthermore, we conducted a detailed study on the effects of shear stress fields and polymeric stress. In this calculation, the coordinates r and z, as well as

time t, were non-dimensionalized using equations (9) ~ (11) as follows. The dimentionless numbers are defined as shown in equations (12) thorough (14). Here, R_m represents the maximum bubble radius attained by a bubble in an infinite expanse of inviscid fluid.

$$r^* = \frac{r}{R_m} \tag{9}$$

$$z^* = \frac{z}{R_m} \tag{10}$$

$$t^* = \frac{t}{R_m}\left(\frac{p_{ref}}{\rho}\right)^{\frac{1}{2}} \tag{11}$$

$$Re = \frac{R_m}{\eta}\left(\left(P_{ref}\right)\rho\right)^{1/2} \tag{12}$$

$$De = \frac{\lambda_1}{R_m}\left(\frac{P_{ref}}{\rho}\right)^{\frac{1}{2}} \tag{13}$$

$$We = \frac{R_m P_{ref}}{\sigma} \tag{14}$$

3.1. Effect of initial standoff distance

The results corresponding to a relaxation time λ_1= 0.02 s are presented below. As for h = 2.0, the fluid flow acted in the upward direction and obliquely downward, contributing to the formation of an interesting shape during the contraction phase as shown in **Fig. 3 – (c) to (f)**. Local concentration of stress on the lateral sides of the bubble resulted from these oblique jet flows, leading to complex deformation. The maximum of T_{nn} at head of the bubble reached approximately 0.1, highlighting the strong nonlinear effects. This behavior is attributed to the weakened influence of the wall, allowing the fluid to deform more freely.

When the bubble was initially positioned closer to the wall (h = 1.0), a vertically downwards jet flow acted from upward, causing the upper side of the bubble to fold inward during the contraction phase. Strong stress distribution was observed at the upper part of the bubble as shown in **Fig. 4**. In particular, negative stress (negative value defined to be in the outward direction from the bubble surface) concentrated locally in the upper deformation region, indicating a pronounced effect of shear stress. The depressed shape at the bubble top was caused by strong elastic effects and closer proximity to the wall.

In the case of h = 4.0, a horizontal jet flows from the sides contributing to the extension in the vertical direction, with local extra stress up to 0.3 at the center during the contraction phase as shown in **Fig. 5**. As a result, the delayed relaxation of polymer stress caused bubble elongation, leading to a bubble shape at the onset of fragmentation. In this case, the wall's influence was smaller, forming a uniform stress field except for necking area.

(a) t^* = 0 (Initial bubble)

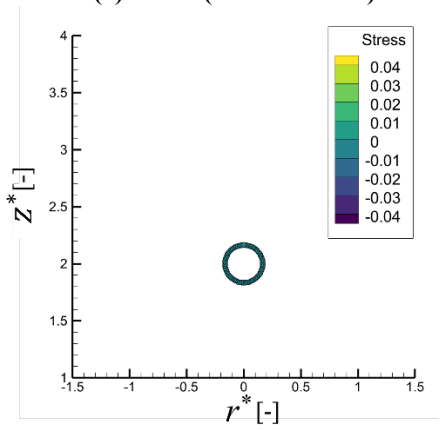

(b) t^*=0.5530 (Expansion phase)

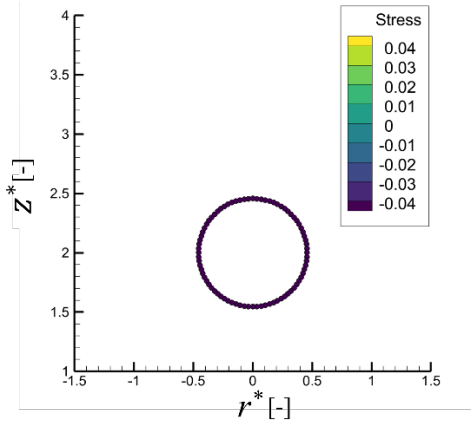

(c) t^*=2.184 (Contraction phase)

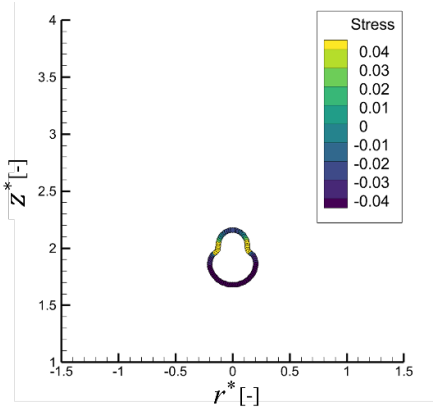

(d) t^*=2.648 (Expansion phase)

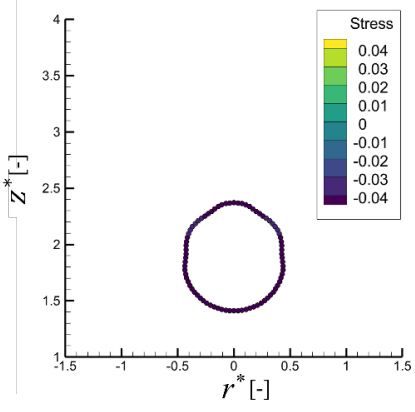

(e) t^*=3.143 (Contraction phase)

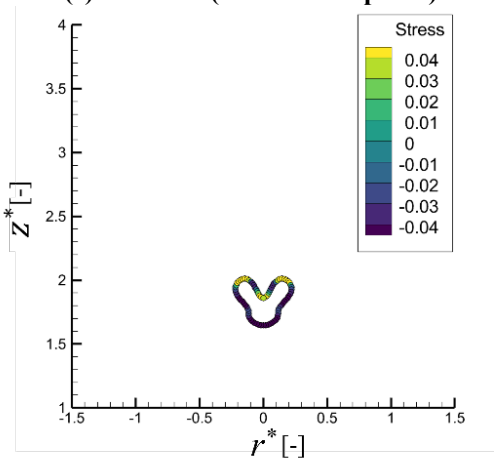

(f) t^*=3.219 (Most contraction phase)

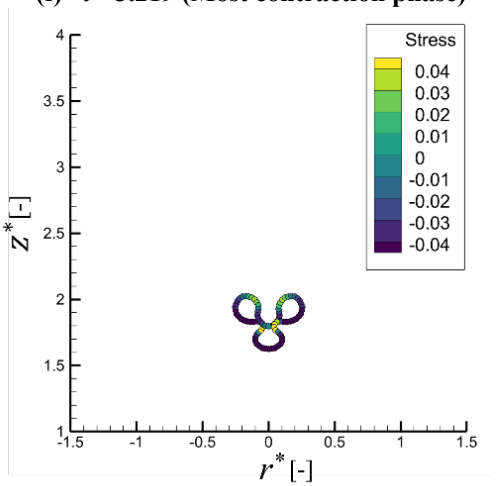

Fig. 3 Profiles of bubble shape and stress distribution in the Giesekus model at h=2.0. (η_0 = 90.49 Pa·s, λ_1 = 0.02 s, σ = 0 mN/m, γ=1.25, α = 0.3, Re = 0.1137, De = 195.2, We^{-1} = 0)

Final shape(t^*=1.100, Contraction phase)

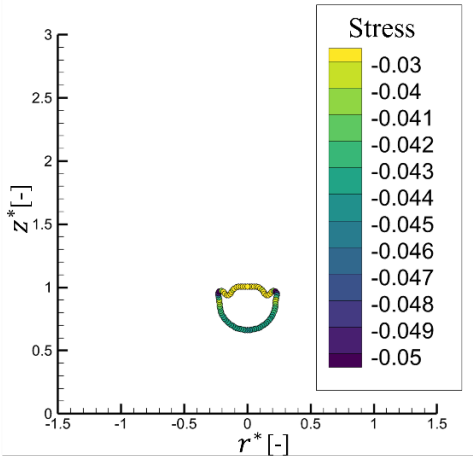

Fig. 4 Profiles of bubble shape and stress distribution in the Giesekus model at h=1.0. (η_0 = 90.49 Pa·s, λ_1 = 0.02 s, σ = 0 mN/m, γ=1.25, α = 0.3, Re = 0.1137, De = 195.2, We^{-1} = 0)

Final shape (t^*=5.191, Contraction phase)

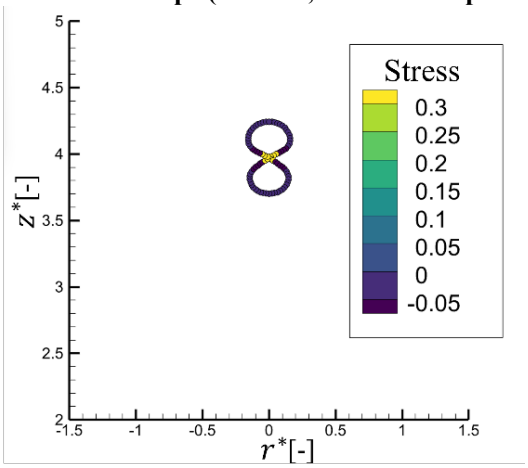

Fig. 5 Profiles of bubble shape and stress distribution in the Giesekus model at h=4.0. (η_0 = 90.49 Pa·s, λ_1 = 0.02 s, σ = 52.5 mN/m, γ=1.25, α = 0.3, Re = 0.1137, De = 195.2, We^{-1} = 0)

3.2. Effect of Surface tension

To help understand the factors which lead to the formation of the various bubble shapes, we examined the effect of surface tension at the bubble surface. The calculations were performed by varying the reciprocal of the Weber number We^{-1}, while keeping the reference pressure of the viscoelastic fluid P_{ref} and the maximum bubble radius R_m constant. When the surface tension is set to zero, i.e., We^{-1} = 0, the results are shown in **Fig. 3**. In contrast, the result for a surface tension σ = 52.5 mN/m, corresponding to a 1 wt% CMC aqueous solution at 25 °C, is presented in **Fig. 9.** In this case, it is observed that the bubble expands and contracts alternately while maintaining its spherical shape. The stress is observed to be uniformly distributed across the entire bubble interface, with no significant local concentration of stress. This is likely occurred because the surface tension helps to maintain the smooth and symmetrical bubble shape. Additionally, the results for near-zero surface tension conditions specifically σ = 0.0725 mN/m and σ = 0.725 mN/m are shown in **Figs. 10** and **11**, respectively. Other unique bubble shapes and significant deformation were observed in both cases. A similar final bubble shape to the zero surface tension case was observed at $We^{-1} = 7.18\times10^{-4}$ as shown in **Fig.10**. The pinch off points can be observed to take place in lateral regions around the bubble, as shown in **Fig.11**.

(a) **Initial bubble (t^*= 0)**

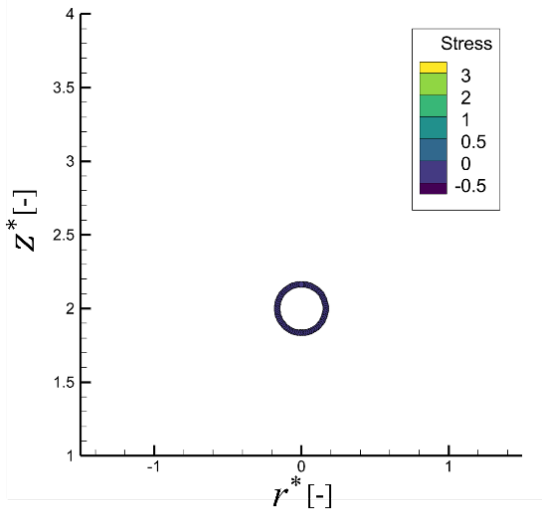

(b) **Expansion phase (t^*= 24.34)**

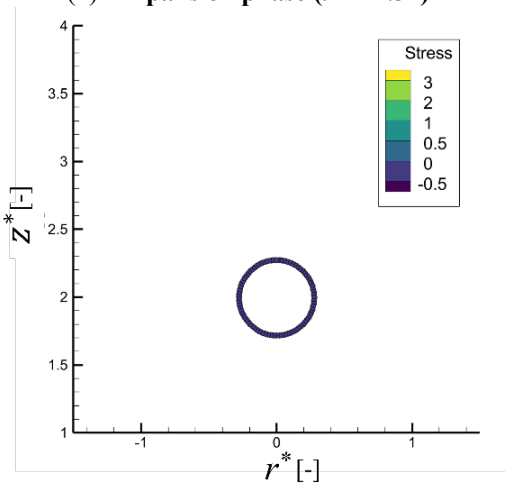

(c) **Final shape (t^*= 84.66, Contraction phase)**

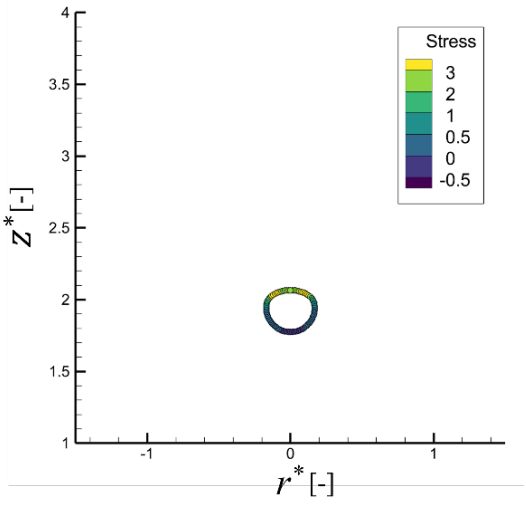

Fig. 9 Profiles of bubble shape and stress distribution in the Giesekus model at h=1.0. (η_0 = 90.49 Pa·s, λ_1= 0.02 s, σ = 52.5 mN/m, γ=1.25, α = 0.3, Re = 0.1137, De = 195.2, We^{-1} = 0.5198)

Final shape (t^*=3.194, Contraction phase)

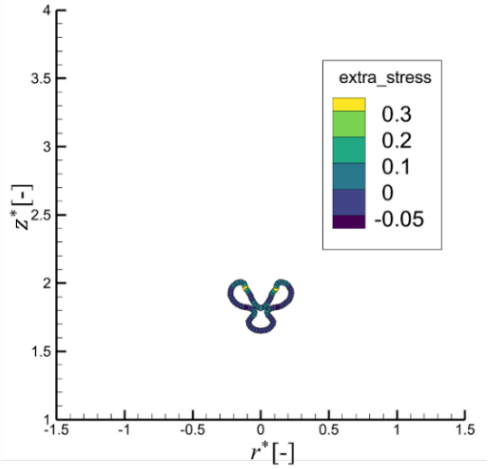

Fig. 10 Profiles of bubble shape and stress distribution in the Giesekus model at h=1.0. (η_0 = 90.49 Pa·s, λ_1=0.02 s, σ = 0.0725 mN/m, γ=1.25, α = 0.3, Re = 0.1137, De = 195.2, We^{-1} = 0.000718)

Final shape (t^*=3.186, Contraction phase)

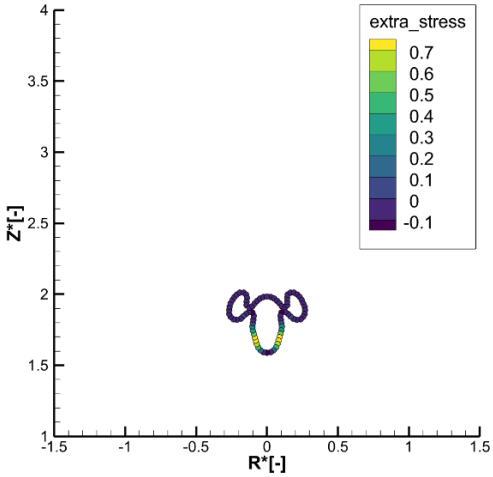

Fig. 11 Profiles of bubble shape and stress distribution in the Giesekus model at h=1.0. (η_0 = 90.49 Pa·s, λ_1= 0.02 s, σ = 0.725 mN/m, γ=1.25, α = 0.3, Re = 0.1137, De = 195.2, We^{-1} = 0.00718)

3.3. Investigation based on Shear rate

For a relaxation time λ_1 = 0.02 s and zero-shear viscosity η_0 = 90.49 Pa·s, the shear rate $\dot{\gamma}$ was calculated using the rate of deformation tensor **S**, defined by following equation (15). Additionally, the shear rate $\dot{\gamma}$ was calculated at the points on the bubble interface where the strongest stress acts during the contraction phase as shown in **Table 1**.

$$\dot{\gamma} = \sqrt{2\mathbf{S}:\mathbf{S}} \qquad (15)$$

$$\mathbf{S} = \frac{1}{2}\left(\nabla\mathbf{u} + \left(\nabla\mathbf{u}\right)^{T}\right) \tag{16}$$

In the case of **Fig.4** (h = 1.0), strong local stress occurred at the upper bubble surface, where the local shear rate at node number k=1 was observed to be up to 687 s^{-1} during the contraction phase. However, a weaker local stress was observed in lower regions with lower local shear rates around 100 s^{-1}.

As for the case of **Fig.3** (h = 2.0), the maximum shear rate was observed at k = 1 during the expansion phase, with a local shear rate of 4.281 s^{-1}. The bubble exhibited an interesting shape during the contraction phase, with the strongest stress acting at the bubble's center. The local shear rate at this point was up to 2960 s^{-1} in the final contraction phase as shown in **Fig.3-(f)**. It can be seen that the bubble is ready to pinch off into three parts.

In the case of **Fig.5** (h = 4.0), the bubble deformed into a vertically contracted shape during the contraction phase, with the strongest stress occurring at k = 21. The local shear rate at this point was 199 s^{-1}.

Table 2 shows the local shear rates under the condition of h = 2.0 as a function of surface tension. Shear rates are extremely higher for all cases during the contraction phase. In the zero-tension case (σ = 0 mN/m), the peak shear rate reaches 2936 s^{-1} at t^*=3.218. Introducing a low surface tension of σ = 0.0725 mN/m reduces this peak by approximately 80% to 522 s^{-1} at the same phase. For σ = 0.725 mN/m, the peak is about 1536 s^{-1}, and the peak is suppressed to just 195s^{-1} at σ = 52.5 mN/m.

Table 1 Details of the local shear rate in the Giesekus model. (η_0 = 90.49 Pa·s, λ_1 = 0.02 s, γ=1.25, α = 0.3)

Height h [-]	Nodal number k [-]	Dimentionless time t^* [-]	Shear rate $\dot{\gamma}$ [s^{-1}]
1.0	1	0.5530 (Expansion phase)	2.88
		1.100 (Contraction phase)	687
2.0	1	0.5530 (Expansion phase)	4.28
		3.218 (Contraction phase)	2960
4.0	21	1.552 (Expansion phase)	0.548
		5.191 (Contraction phase)	199

Table 2 Details of local shear rate in the Giesekus model due to differences in surface tension at the bubble surface. (η_0 = 90.49 Pa·s, λ_1 = 0.02 s, γ=1.25, α = 0.3)

Height h [-]	Surface tension σ [mN/m]	Nodal number k [-]	Dimentionless time t^* [-]	Shear rate $\dot{\gamma}$ [s^{-1}]
2.0	0	1	0.5530 (Expansion phase)	4.28
			3.218 (Contraction phase)	2960
2.0	0.0725	1	0.5527 (Expansion phase)	1.82
			3.186 (Contraction phase)	522
2.0	0.725	1	0.5529 (Expansion phase)	1.82
			3.194 (Contraction phase)	1536
2.0	52.5	1	24.34 (Expansion phase)	2.72
			84.66 (Contraction phase)	195

CONCLUSIONS

We performed a numerical simulation to analyze the expansion and contraction behavior of a bubble placed near a rigid wall in a viscoelastic fluid using the Giesekus model (α = 0.3).

It was found that the deformation of the bubble varied significantly depending on the initial distance between the bubble and the rigid wall. This is due to the combined influence of the restricted fluid movement near the wall and the rheological properties of the viscoelastic fluid, which together influence the deformation of the bubble. Moreover, the results indicate that surface tension significantly affects the morphology of the bubble.

ACKNOWLEDGEMENTS

This work was supported by JSPS KAKENHI Grant Numbers (20K04285 and 23K03673) from the Japan Society for Promotion of Science (JSPS).

REFERENCES

[1] S. Iwata et al., 2008, "Pressure-oscillation deforming for viscoelastic fluid," *Journal of Non-Newtonian Fluid Mechanics*, Vol.151(1-3), pp.30-37.

[2] S. Ito et al., 2020, "Numerical simulation of a rising bubble in a shear-thinning fluid under pressure-oscillating field," *Nihon Reoroji Gakkaishi*, Vol.48, No.3, pp.145-151.

[3] Lind, S.J. and Phillips, T.N., 2012. The influence of viscoelasticity on the collapse of cavitation bubbles near a rigid boundary. *Theoretical and Computational Fluid Dynamics*, *26*, pp.245-277.

[4] Joseph, D.D. and Liao, T.Y., 1994. Potential flows of viscous and viscoelastic fluids. *Journal of Fluid Mechanics*, *265*, pp.1-23.

[5] M.J.Walters et al., 2015, "An Investigation into the Effects of Viscoelasticity on Cavitation Bubble Dynamics with Applications to Biomedicine,", Cardiff University